Biomedical Signal Processing and Control 30 (2016) 31–42

Contents lists available at ScienceDirect

Biomedical Signal Processing and Control

journal homepage: www.elsevier.com/locate/bspc

Heart rate control during treadmill exercise using input-sensitivity shaping for disturbance rejection of very-low-frequency heart rate variability

Kenneth J. Hunt*, Simon E. Fankhauser

Institute for Rehabilitation and Performance Technology, Division of Mechanical Engineering, Department of Engineering and Information Technology, Bern University of Applied Sciences, CH-3400 Burgdorf, Switzerland

ARTICLE INFO

Article history:
Received 9 March 2016
Received in revised form 30 May 2016
Accepted 20 June 2016

Keywords:
Feedback control
Heart rate
Treadmill exercise
Frequency response
Physiological control

ABSTRACT

Background: Automatic and accurate control of heart rate (HR) during treadmill exercise is important for prescription and implementation of training protocols. The principal design issue for feedback control of HR is to achieve disturbance rejection of very-low-frequency heart rate variability (VLF-HRV) with a level of control signal activity (treadmill speed) which is sufficiently smooth and acceptable to the runner. This work aimed to develop a new method for feedback control of heart rate during treadmill exercise based on shaping of the input sensitivity function, and to empirically evaluate quantitative performance outcomes in an experimental study.

Methods: Thirty healthy male subjects participated. 20 subjects were included in a preceding study to determine an approximate, average nominal model of heart rate dynamics, and 10 were not. The design method guarantees that the input sensitivity function gain monotonically decreases with frequency, is therefore devoid of peaking, and has a pre-specified value at a chosen critical frequency, thus avoiding unwanted amplification of HRV disturbances in the very-low-frequency band. Controllers were designed using the existing approximate nominal plant model which was not specific to any of the subjects tested.

Results: Accurate, stable and robust overall performance was observed for all 30 subjects, with a mean RMS tracking error of 2.96 beats/min and a smooth, low-power control signal. There were no significant differences in tracking accuracy or control signal power between the 10 subjects who were not in the preceding identification study and a matched subgroup of subjects who were (respectively: mean RMSE 2.69 vs. 3.28 beats/min, $p = 0.24$; mean control signal power 15.62 vs. 16.31×10^{-4} m^2/s^2, $p = 0.37$). Substantial and significant reductions over time in RMS tracking error and average control signal power were observed.

Conclusions: The input-sensitivity-shaping method provides a direct way to address the principal design challenge for HR control, namely disturbance rejection in relation to VLF-HRV, and delivered robust and accurate tracking with a smooth, low-power control signal. Issues of parametric and structural plant uncertainty are secondary because a simple approximate plant model, not specific to any of the subjects tested, was sufficient to achieve accurate, stable and robust heart rate control performance.

1. Introduction

The ability to automatically and accurately control heart rate (HR) during treadmill exercise would bring important benefits for the prescription and implementation of exercise training protocols. Heart rate is used to delineate the exercise intensity regimes which form part of current recommendations for development and maintenance of cardiorespiratory fitness [1]; these recommendations are given in terms of frequency, duration and intensity, the latter typically lying in the range of "moderate" to "vigorous" exercise. Exercise intensity, in turn, is described as a percentage of either maximal heart rate (HR_{max}) or of heart rate reserve (HRR), which is the difference between maximal and resting heart rates: $HRR \triangleq HR_{max} - HR_{rest}$. Using HRR, moderate and vigorous intensities correspond respectively to the ranges 40–59% and 60–89% of HRR [2].

High-intensity interval training (HIT), which combines periods of vigorous to high-intensity exercise with low or moderate-intensity recovery periods, has been shown to provide additional

* Corresponding author.
E-mail addresses: kenneth.hunt@bfh.ch (K.J. Hunt), sfanky_1990@bluewin.ch (S.E. Fankhauser).

http://dx.doi.org/10.1016/j.bspc.2016.06.005

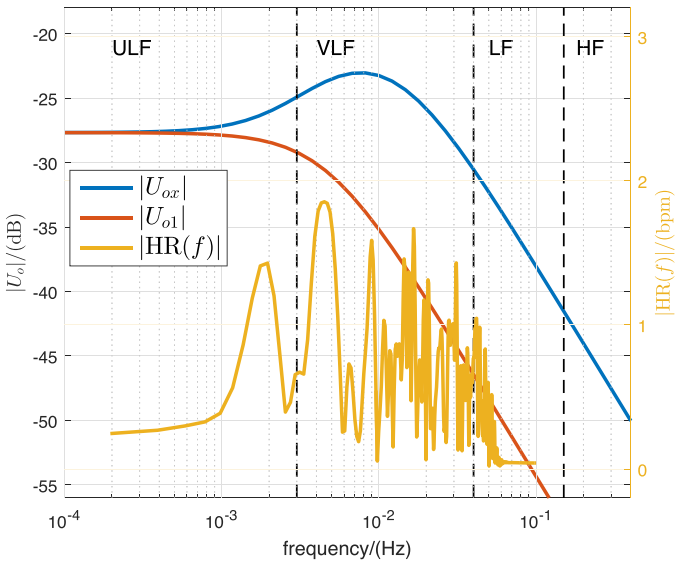

Fig. 1. Four principal frequency bands for heart rate variability analysis: ultra-low frequency (ULF), very-low frequency (VLF), low frequency (LF) and high frequency (HF). Amplitude spectrum of HR for subject S02 (orange trace, right-hand y-axis). Input sensitivity function magnitudes $|U_o(j\omega)|$ (left-hand y-axis) for naive feedback design (blue trace $|U_{ox}|$) and for shaped controller C_1 (red trace $|U_{o1}|$; Eqs. (33) and (34)). (For interpretation of the references to colour in this legend, the reader is referred to the web version of the article.)

benefits for cardiorespiratory fitness and cardiovascular function when compared to constant-intensity training (systematic reviews: [3,4]). There is considerable flexibility in setting the durations and intensity levels of the different regimes within HIT in healthy adults [3] and in various patient groups, e.g. in cardiac rehabilitation [5]. This motivates the development of accurate and robust feedback approaches for automatic control of arbitrary heart rate reference profiles. For treadmill-based training, the feedback controller would automatically adjust the treadmill speed based on continuous observation of the reference and actual HR values.

The primary design challenge for feedback control of heart rate is to ensure that the control system maintains acceptable performance in the face of disturbances to the heart rate caused by physiological heart rate variability (HRV) [6]; this concept is supported by data presented in the preliminary observational case study below. Performance of heart rate control systems should always be quantified in terms of both tracking accuracy (e.g. root-mean-square heart-rate tracking error, RMSE) and the level of activity of the control signal (e.g. average power of the control signal, i.e. the treadmill speed reference). For the HR control application, the classical trade-off between tracking accuracy and control signal power – higher accuracy is usually achieved at the cost of increased control signal activity – is particularly pronounced and important: the HRV disturbance entering the system will be rejected to a degree defined by the frequency-response of the sensitivity function (S_o, Eq. (11)), with a higher level of disturbance rejection leading generally to lower tracking error but requiring higher control signal power. Since the control signal in this case is the treadmill speed reference, changes in this variable directly impact on the human subject running on the treadmill, so these changes must be kept within acceptable limits, even if some degree of tracking accuracy has to be sacrificed; hence the importance of the input sensitivity function (U_o, Eq. (12)), which links the HRV disturbance to the control signal.

Current standards for measurement and interpretation of HRV identify four principal frequency bands for analysis [7,8] (cf. Fig. 1):

- ultra-low frequency (ULF), with frequency $f < 0.003$ Hz;
- very-low frequency (VLF), where $0.003 \le f < 0.04$ Hz;
- low frequency (LF), $0.04 \le f < 0.15$ Hz;
- high frequency (HF), $0.15 \le f \le 0.4$ Hz.

For design of heart rate controllers, the VLF component is of primary importance because this band usually incorporates the crossover region of the feedback loop; peaking of the sensitivity functions can occur in the crossover region, potentially leading to unwanted power in the control signal in the VLF frequency band, which manifests as changes in the treadmill speed which would be strongly perceptible to the runner. HRV in the ULF band, in contrast, represents a very slow disturbance which can readily be fully rejected by having high gain in the controller in this range (e.g. by using integral action); the resulting very-slow changes in the control signal would not be perceived as unpleasant or undesirable by the runner – the upper-frequency bound of the ULF range, 0.003 Hz, corresponds to an oscillation period of just over 5 min (333.3 s). HRV in the LF and HF frequency bands, on the other hand, will typically lie outwith the bandwidth of the feedback loop and will have little effect on the control signal if the controller's frequency response is appropriately designed; one way to do this is to prescribe a strictly-proper controller transfer function so that the loop gain rolls off towards zero above the crossover region. This makes the control signal insensitive to HRV disturbances in the LF and HF bands.

These considerations emphasize that the feedback loop properties in the VLF band are paramount and that disturbance rejection behaviour is the key design issue; these concepts are further elucidated in the case presented in Section 2. To directly address these challenges, a novel design approach is derived and tested in the present work which is based on shaping the frequency response of the input sensitivity function (U_o, Eq. (12): the transfer function between the HRV disturbance and the control signal) so that it has a pre-specified gain at a selected critical frequency in the crossover region within the VLF band. Moreover, the design approach is constrained to make the gain of the input sensitivity function monotonically decreasing with frequency, so that peaking of this gain cannot occur. Finally, the requirements of the ULF and LF/HF bands are addressed respectively, as alluded to above, by including integral action in the feedback compensator and by making it strictly proper (i.e. low pass).

Previous work on treadmill HR control has focused not on the key issues of HRV and disturbance rejection, but rather on parametric and structural plant uncertainty [9–12]. A further novel element of the present work is the assumption of a very simple and approximate model of heart rate dynamics, which was the outcome of a companion identification study [13]. The control design approach detailed here uses this single approximate nominal plant model, and does not require any information on, or identification of, heart rate dynamics for individual runners. A similar nominal model strategy was taken in related reports of heart rate control during outdoor running [14] and in a comparison of linear and nonlinear heart rate controllers [15].

The aim of the present work was twofold: to set out the input-sensitivity-shaping method for feedback control of heart rate during treadmill exercise; and to empirically evaluate quantitative performance outcomes with the proposed method in an experimental study with a number of subjects sufficient to allow statistically valid conclusions to be drawn.

2. HRV – preliminary observational case study

The introductory discussion highlighted the importance of the VLF band of HRV for the design of HR control systems, and that disturbance rejection is the principal design issue. These concepts can be exemplified by considering data recorded from one

of the subjects who participated in the present study (subject S02, Figs. 1 and 2).

Spectral analysis of this subject's HR, obtained using FFT analysis of raw ECG data recorded during a 20-min period of constant-speed, vigorous-intensity running, showed that HRV power was concentrated primarily within the VLF frequency band (Fig. 1). When this subject's HR was controlled using a naive feedback design with substantial peaking of the input sensitivity function (blue trace $|U_{ox}|$ in Fig. 1), very strong and wholly unacceptable variation of the treadmill speed was observed at a dominant frequency corresponding closely to the frequency of the resonant peak of the input sensitivity function during both reference tracking (Fig. 2(a)) and steady-state regulation (Fig. 2(c)): the peak value of $|U_{ox}|$ is 0.07 (−23 dB) at a frequency of 0.008 Hz (Fig. 1); the control signal (lower plots in Fig. 2(a) and (c)) can be seen to be oscillating at a frequency of about 0.01 Hz (e.g. there are about 10 clearly-identifiable peaks in the time range $600 \le t \le 1600$ s in the lower plot of Fig. 2(c)).

Moreover, the ratio of the peak-to-peak amplitudes of the control signal oscillation and the principal component of HRV corresponds closely to the peak gain of the input sensitivity function $|U_{ox}|$, which was identified above as 0.07 (−23 dB): considering the half-period following $t = 820$ s in Fig. 2(c), a rise in HR of about 11 bpm was seen, resulting in a change in speed of about 0.79 m/s, giving a gain of 0.79/11 = 0.07. These oscillations were apparently driven by both the step changes in the reference signal (Fig. 2(a)) and by the VLF component of HRV (Fig. 2(c)); this is as expected, since the input sensitivity function links both the reference and the disturbance to the control signal (cf. Eq. (12)).

When a controller was employed which was designed using the proposed input-sensitivity-shaping approach (Section 4), denoted as controller C_1, where the gain of the input sensitivity function at the critical frequency 0.01 Hz within the VLF band was pinned down to a value which was one quarter of the value determined for the naive controller above, i.e. 0.0174 (−35.19 dB, red trace $|U_{o1}|$ in Fig. 1), and no peaking was permitted, oscillation of the control signal was eliminated (Fig. 2(b) and (d), lower plots). For this example, the LF and HF bands for HRV lie well above the closed-loop bandwidth (Fig. 1). ULF variability, on the other hand, is seen to be eliminated appropriately by integral action, apparent through the ultra-slow, decreasing trend for treadmill speed over time in each of the tests.

With this controller, C_1, it can again be seen that the ratio of the observed peak-to-peak amplitudes of the control signal and the principal component of HRV corresponds closely to the chosen peak

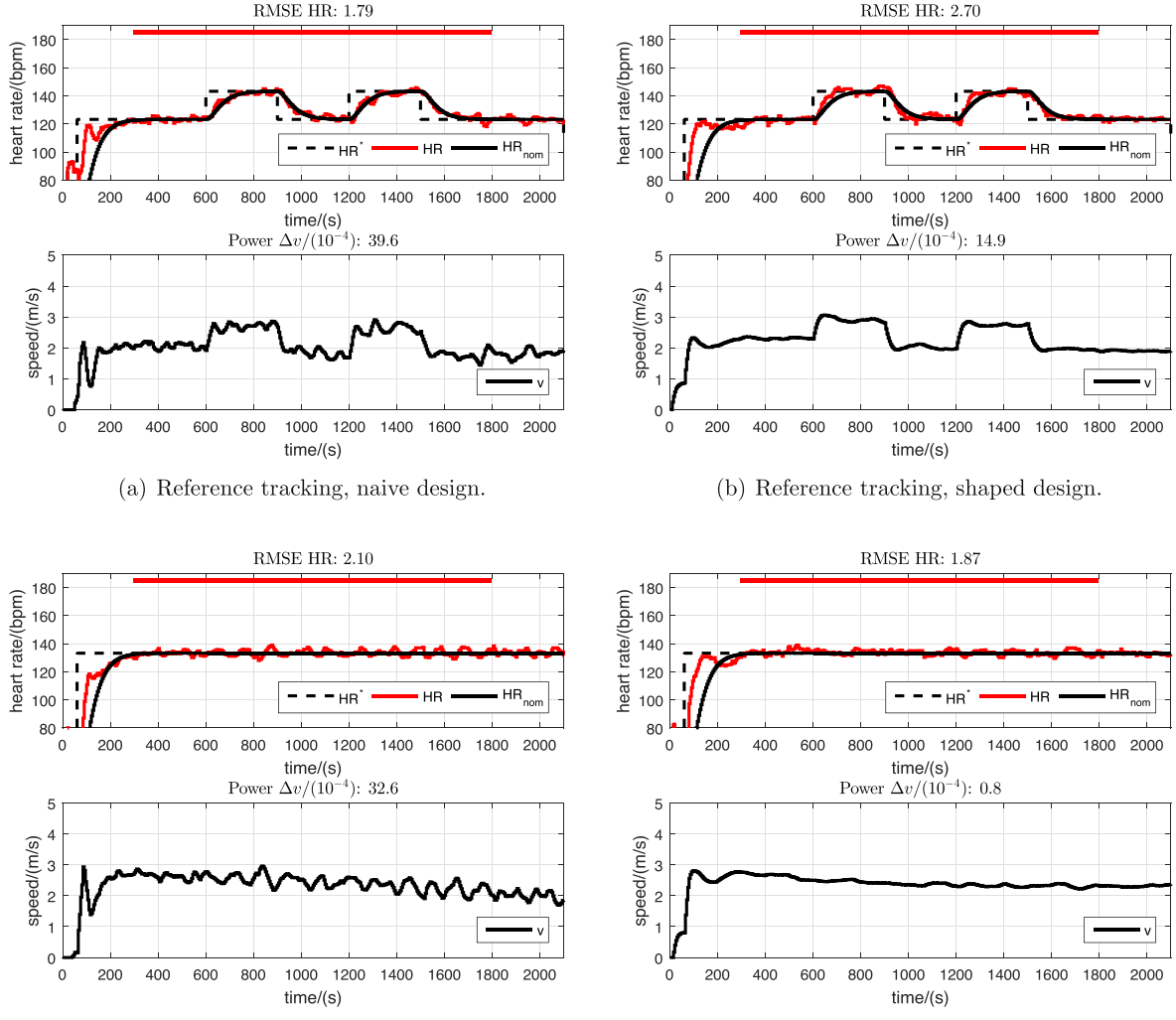

(a) Reference tracking, naive design.

(b) Reference tracking, shaped design.

(c) Constant-reference regulation, naive design.

(d) Constant-reference regulation, shaped design.

Fig. 2. Illustrative example – HR control measurements with subject S02. Left column: reference tracking (a) and constant-reference regulation (c) using naive design with peaking input sensitivity function U_{ox}. Right column: reference tracking (b) and constant-reference regulation (d) using input-sensitivity-shaped controller C_1, U_{o1}. In the upper part of each figure, HR* is the heart rate reference, HR_{nom} is the target nominal heart rate response (simulated), and HR is the measured heart rate. In the lower graphs, v is the control signal, i.e. the treadmill speed reference. RMSE: root-mean-square tracking error, Eq. (5). Power $P_{\Delta v}$: average control signal power, Eq. (6).

Table 1
Subject characteristics.

	Mean (SD)	Range
Age/(y)	28.4 (10.1)	18–57
Body mass/(kg)	75.3 (9.9)	60–101
Height/(m)	1.77 (0.07)	1.63–1.93
BMI/(kg/m^2)	24.0 (2.5)	19.6–30.2

$n = 30$, all male.
SD: standard deviation.
BMI: body mass index; BMI = mass/height^2.

gain of the input sensitivity function, viz. $|U_{o1}|_{f=0.01} = 0.0174$: the maximum peak-to-peak change in HR during the tests with C_1 was ~10 bpm (Fig. 2(b) and (d), upper plots); analysis of the time period $1625 \le t \le 1725$ s during the regulation test (Fig. 2(d)), where the largest change in speed during this test occurred, gave a change in speed of 0.174 m/s. Thus the observed gain was 0.174/10 = 0.0174. This magnitude of change in speed in response to the largest observed variation in heart rate around the critical frequency of 0.01 Hz was barely perceptible to the runner. The critical gain and frequency values given by $|U_{o1}|_{f=0.01} = 0.0174$ were therefore taken forward for full experimental evaluation of controller C_1 as detailed in the sequel.

3. Experimental methods

3.1. Subjects and ethics

Thirty healthy males participated in the study (details – Table 1). Of these 30 subjects, 20 had taken part in a preceding study [13] to determine an approximate, average nominal model of heart rate dynamics, and 10 had not. The study was approved by the local ethics committee (Ethics Committee of the Swiss Canton of Bern, Ref. KEK-Nr. 313/14) and subjects provided written, informed consent during recruitment. The primary inclusion/exclusion criteria were: healthy males from 18 to 60 years of age, and absence of muscular, orthopaedic or cardiovascular issues contraindicating vigorous treadmill exercise. Prior to each test, subjects were required to avoid strenuous exercise, alcohol and smoking (all 24 h in advance), and also heavy meals (4 h) and caffeine (12 h).

3.2. Apparatus

A computer-controlled treadmill was employed (model Venus, h/p/cosmos Sports and Medical GmbH, Germany) connected by an RS-232 serial communication link to a PC (Fig. 3). The heart rate controllers were implemented in the PC using Matlab/Simulink and the associated Real Time Workshop (The Mathworks, Inc., USA).

Controllers were designed in the continuous-time domain (Section 4) and implemented digitally using a sample interval of $T_s = 5$ s. This choice of T_s was based on the recommendation of having ~4–10 samples per rise time of the plant [16] – the nominal plant model had a time constant τ of 57.6 s (Eq. (1), Section 3.3), but this nominal time constant is an average obtained over 48 individual models, where individual values were seen to be as low as τ =27.3 s [13].

Heart rate was measured using a chest belt (model T34, Polar Electro Oy, Finland) and three associated wireless receivers arranged in a triangle configuration with respect to the treadmill surface, and integrated with the treadmill hardware control unit. Heart rate was transmitted from the treadmill to the PC via the serial link and read into the simulink real-time control model at the rate of 1 Hz. At each controller sample instant, i.e. every 5 s, the 5 heart rate samples obtained in the preceding 5-s sample interval were averaged and fed into the control loop.

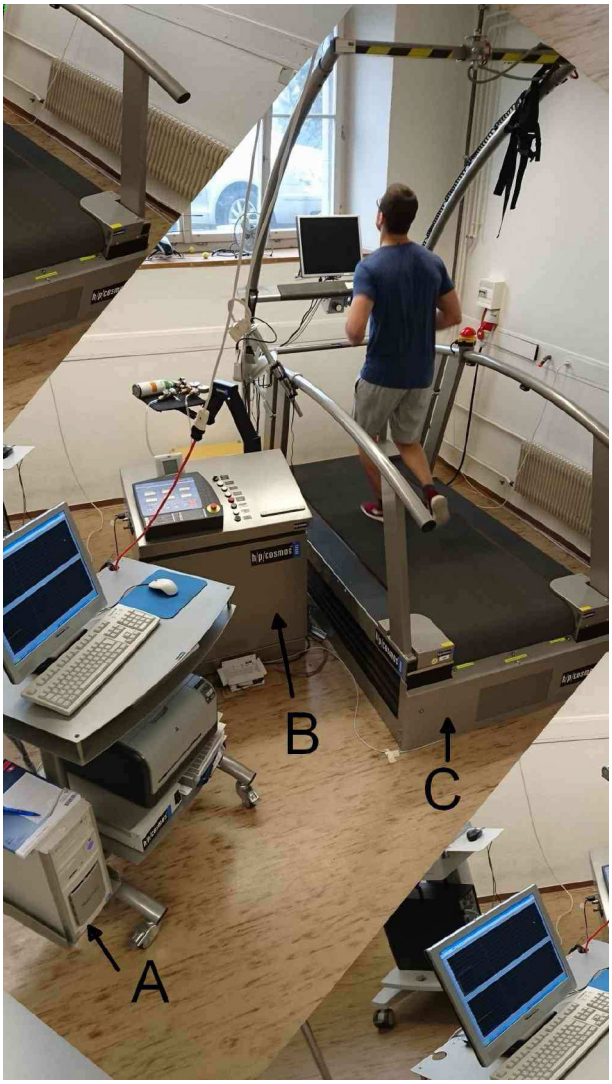

Fig. 3. Experimental setup showing the PC in which the real-time heart rate controllers were implemented (A), the treadmill control unit (B) and the treadmill (C).

3.3. Approximate nominal plant model and control approach

Feedback control design utilised an approximate nominal model P_o of the dynamic response between the treadmill speed reference signal v and heart rate HR [13]:

$$v \to \text{HR}: \quad P_o(s) = \frac{k}{\tau s + 1} = \frac{24.2}{57.6s + 1}, \tag{1}$$

where k is the steady-state gain and τ is the time constant of this first-order model structure. The nominal plant parameter $k = 24.2$ bpm/(m/s) and $\tau = 57.6$ s were obtained in the previous study as averages of 48 individual models which were empirically identified from 24 healthy male subjects who each ran, in separate identification tests, at moderate and vigorous intensities, thus giving 24 subjects × 2 models/subject = 48 models in total [13].

The structure employed here for heart rate control comprised a feedback compensator C and a reference prefilter C_{pf} (Fig. 4). The signal HR* is the heart rate reference, v is the treadmill speed reference, which serves as the plant control input, and d is a disturbance. r' and e' are intermediate signals which are used in the analysis that follows (Section 4).

The feedback compensator C was designed using the input-sensitivity-shaping methodology detailed in the sequel (Section 4),

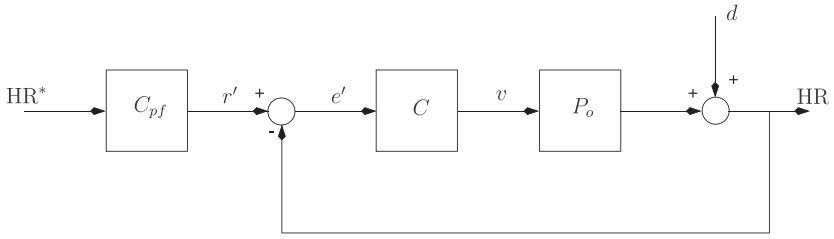

Fig. 4. Control structure: C is the feedback compensator and C_{pf} is a reference prefilter. The principal signals in this structure are the heart rate reference HR*, the actual heart rate HR, the treadmill speed reference v (plant control input), and a disturbance d which mainly represents heart rate variability.

while the reference prefilter C_{pf} was separately designed to set the dynamics of the HR reference tracking response.

Following the terminology and notation used classically by Kwakernaak [17], the input sensitivity function, denoted U_o, is defined as the transfer function from the disturbance d to the plant control input v:

$$d \to v: \quad U_o(s) = \frac{C(s)}{1 + C(s)P_o(s)}. \tag{2}$$

In the present context of heart rate control, the disturbance signal d is taken to represent natural, but unpredictable, changes in heart rate stemming from physiological heart rate variability.

The key idea of the input-sensitivity feedback design method (details in Section 4) is to shape the frequency response of the input sensitivity function such that its gain $|U_o(j\omega)|$ has a specified nominal value at a given critical frequency, and, moreover, such that $|U_o(j\omega)|$ is monotonically decreasing with frequency so that peaking cannot occur. These measures are intended to ensure that heart rate variability does not lead to an unacceptable level of activity in the treadmill speed around the critical frequency. Two different controllers were tested, denoted C_1 and C_2 (Section 4.5), where C_2 had a gain which was +4 dB higher (i.e. higher by an absolute factor of ~1.6) than C_1 at the chosen critical frequency.

The reference prefilter C_{pf} was separately designed to set the dynamics of the HR reference tracking to an overall closed-loop transfer function T_{cl}, which had the form of the standard second-order transfer function:

$$\text{HR}^* \to \text{HR}: \quad T_{cl}(s) = \frac{\omega_n^2}{s^2 + 2\zeta\omega_n s + \omega_n^2}, \tag{3}$$

where ζ is the relative damping and ω_n is the undamped natural frequency of oscillation.

Considering the control structure employed (Fig. 4), the designated overall closed-loop transfer function is obtained by setting the prefilter to

$$C_{pf} = T_{cl} \cdot T_o^{-1}, \tag{4}$$

where T_o, the complementary sensitivity function (see Eq. (10)), is the transfer function from r' to HR.

For all controller tests, ζ was set to the critical value $\zeta = 1$ while ω_n was obtained from a chosen 10–90% closed-loop rise time t_r as $\omega_n = 3.35/t_r$, which is the approximation valid around $\zeta = 1$ [18, p. 196]. In all tests, the rise time was set to $t_r = 120$ s.

3.4. Testing protocol

All tests were carried out according to a systematic protocol (Fig. 5): subjects first warmed up for 10 min at a moderate intensity; a 10 min rest followed; then there was a formal measurement phase lasting 35 min; finally, there was a 10 min cool down of running at low intensity. Prior to the warm up of their first test, resting heart rate HR_{rest} was obtained for each subject by manual palpation at the wrist after they had lain resting for 5 min. Estimates of maximal heart rate were set to $\text{HR}_{\text{max}} = 220 - \text{age}$ (cf. [19]).

Following each test, the quantitative outcome measures (RMS tracking error, RMSE, and average control signal power, $P_{\Delta v}$, Eqs. (5) and (6), Section 3.5) were calculated over an evaluation period of $300 \le t \le 1800$ s. During the evaluation period, the heart rate reference HR* was varied by ±10 bpm around a mid level. The mid level was individually set for each subject using 70% of their own heart rate reserve (HRR) to the value $\text{HR}_{70\%} \triangleq 0.7(\text{HR}_{\text{max}} - \text{HR}_{\text{rest}}) + \text{HR}_{\text{rest}}$. The heart rate reference thus changed in a square-wave format every 5 min as $\text{HR}^* = \text{HR}_{70\%} \pm 10$ (Fig. 5). The cool down was at 15 bpm below the individual lower level of the evaluation period, viz. $\text{HR}_{70\%} - 25$.

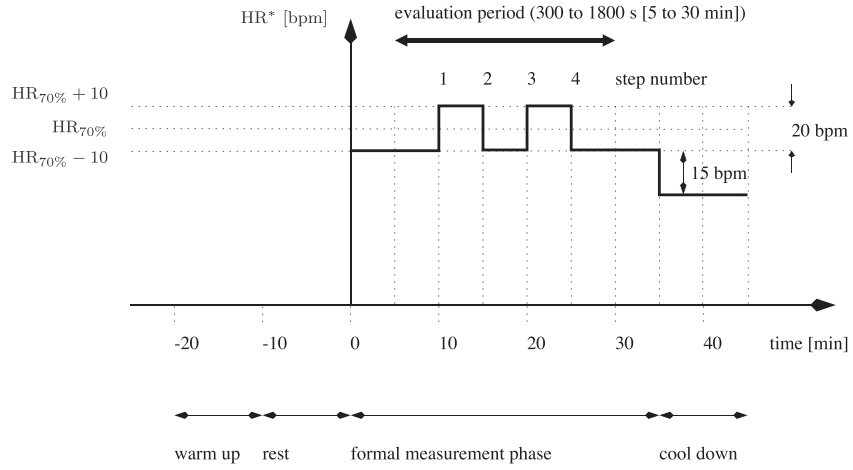

Fig. 5. Measurement protocol.

3.5. Primary outcome measures

Closed-loop control performance was quantitatively assessed using the root-mean-square tracking error (RMSE) for the heart rate, and the average power of changes in the control signal v ($P_{\Delta v}$), where v is the treadmill speed reference.

RMSE was evaluated on an interval $[i_1, i_2]$ corresponding to the evaluation period $300 \le t \le 1800$ s (Fig. 5), where i denote the discrete sample indices, as:

$$\mathrm{RMSE} = \sqrt{\frac{1}{N}\sum_{i=i_1}^{i_2}(\mathrm{HR}_{\mathrm{nom}}(i) - \mathrm{HR}(i))^2} \tag{5}$$

with $N = i_2 - i_1 + 1$. $\mathrm{HR}_{\mathrm{nom}}$ is the target nominal heart rate response which was obtained by simulating the nominal closed-loop transfer function T_{cl} for $\mathrm{HR}^* \to \mathrm{HR}$ (Eq. (3), Fig. 4), i.e. $\mathrm{HR}_{\mathrm{nom}} = T_{cl}\mathrm{HR}^*$.

The intensity of the control signal was characterised as the average power of changes in v over the same interval:

$$P_{\Delta v} = \frac{1}{N-1}\sum_{i=i_1+1}^{i_2}(v(i) - v(i-1))^2, \tag{6}$$

which is often referred to in the sequel for simplicity as "average control signal power."

3.6. Experimental design and statistical analysis

All 30 subjects were tested with controller C_1; the primary outcomes RMSE and $P_{\Delta v}$ are presented using descriptive statistics ($n = 30$).

To determine whether prior participation in the identification study [13] had any influence on the outcomes – 20 of the 30 subjects in the present study belonged to the group of 24 subjects whose individual models were used to determine the average nominal model – a comparative sub-analysis was carried out where the 10 subjects in the present study who had not been in the identification study were paired to 10 of the 20 who had been by matching according to age and BMI. Paired two-sided hypothesis tests were applied to the matched groups of 10 subjects ($n = 10$) to determine whether any significant differences existed in the outcomes RMSE and $P_{\Delta v}$. The null hypothesis for this analysis was that there were no differences in outcomes between the two groups, which are referred to below as "C_1 ID" and "C_1 no ID".

A second comparative analysis was carried out on the outcomes with controllers C_1 and C_2, where C_2 had an additional +4 dB of gain in the input sensitivity function U_o at the critical frequency ω_c (Section 3.3), and also, therefore, a higher bandwidth (Section 4.5). For this analysis, 10 of the 30 subjects were tested with C_2 in addition to having been tested with C_1. Paired one-sided hypothesis tests ($n = 10$) were applied to the outcomes RMSE and $P_{\Delta v}$ to test the expectation, given the higher bandwidth and critical gain, that C_2 would lead to more accurate heart rate tracking (i.e. lower RMSE), but with the cost of higher control signal power (higher $P_{\Delta v}$). The null hypothesis here was that C_2 did not lead to these differences in outcomes.

Two further sub-analyses were carried out for controller C_1 to explore any dependencies in the outcomes RMSE and $P_{\Delta v}$ on time, both for steady-state regulation and for dynamic reference tracking. For steady-state regulation (all subjects, $n = 30$), the outcomes were calculated and compared for two periods of constant reference tracking: "early", where $300 \le t \le 600$ (5–10 min); and "late", where $1800 \le t \le 2100$ (30–35 min); (cf. Fig. 5). Paired two-sided hypothesis tests ($n = 30$) were used to determine whether any significant differences existed in the outcomes for these two time periods, the null hypothesis being that no differences existed.

The data used in the above hypothesis tests were check for normality using a Kolmogorov–Smirnov test with Lilliefors significance correction. t-tests were applied when the hypothesis of normality was not rejected, and Wilcoxon signed rank tests otherwise.

The second analysis of possible time dependency evaluated and compared the outcomes RMSE and $P_{\Delta v}$ for the four individual dynamic step changes in heart rate reference at times $t = 600$, 900, 1200 and 1500, whereby the step number $\in \{1, 2, 3, 4\}$ served as a proxy to the single factor of time (Fig. 5). For each step, the outcomes were calculated over the 300-s time interval following the step onset. This analysis used one-way repeated-measures analysis of variance (ANOVA) with step number as the factor. When significance was determined, post-hoc pairwise comparisons with Bonferroni correction were carried out on all step-number pairs. The null hypothesis was that there were no differences in outcomes between the individual steps. This individual step analysis was done with $n = 29$ because one subject (S22) was found to have an abnormally high RMSE for step 2 (cf. Fig. 7(c), upper graph, step 2): this RMSE lay outwith 3 standard deviations of the mean RMSE across all subjects for step 2 and was therefore considered to be an outlier, and S22 was excluded from this part of the analysis.

The significance level for all hypothesis tests was set at 5% ($\alpha = 0.05$). Paired hypothesis tests were carried out using the Matlab Statistics and Machine Learning Toolbox (The Mathworks, Inc.) and the ANOVAs with SPSS software (IBM Corp., USA).

4. Input sensitivity shaping

The input-sensitivity shaping approach developed here allows the gain of the input sensitivity function U_o to be set to a desired, pre-specified value g_c at a chosen critical frequency ω_c, i.e. it is required that $|U_o(j\omega_c)| = g_c$. Further, U_o is purposely structured so that $|U_o(j\omega)|$ is a monotonically decreasing function of frequency ω and therefore devoid of peaking. By this means, an acceptable nominal amplification/attenuation of the heart rate variability disturbance around the critical frequency within the VLF band can be set by choosing the primary feedback design parameter g_c.

The derivation is given first for the case of a general nominal plant $P_o = B_o/A_o$, i.e. with no restriction on the order of the system (Section 4.1), and then specialised to the first-order case, $n_a = 1$ (Section 4.2).

We consider a control structure with feedback compensator C and reference prefilter C_{pf} (Fig. 4). The input-sensitivity approach pertains only to the feedback element C, while the prefilter C_{pf} is designed separately to give the required reference tracking dynamics (Section 3.3).

4.1. General case

The plant is described by the strictly proper linear transfer function P_o:

$$v \to \mathrm{HR}: \quad P_o(s) = \frac{B_o(s)}{A_o(s)}, \quad n_b < n_a, \tag{7}$$

where n_a and n_b are the respective degrees of the plant denominator and numerator polynomials A_o and B_o. The strictly proper condition reflects the low-pass character of the plant transfer function, since $n_b < n_a \Leftrightarrow \lim_{\omega\to\infty} |P_o(j\omega)| = 0$.

We seek a strictly proper compensator transfer function C, described in rational form by

$$e' \to v: \quad C(s) = \frac{G(s)}{H(s)}, \quad n_g < n_h. \tag{8}$$

C is assumed henceforth to be normalised such that H is monic. The strictly proper condition for C is a design choice which ensures high-frequency rolloff in the compensator (because $n_g < n_h \Leftrightarrow$

$\lim_{\omega\to\infty}|C(j\omega)| = 0$) and, therefore, in the input sensitivity function U_o also, thus making the loop insensitive to high-frequency disturbance components. The compensator is further constrained to have integral action by including the factor s in H via $H(s) = sH'(s)$, giving

$$C(s) = \frac{G(s)}{sH'(s)}, \quad n_g < n_{h'} + 1, \tag{9}$$

where the integrator results in $\lim_{\omega\to 0}|C(j\omega)| = \infty$, i.e. the compensator has infinite steady-state gain.

Inspection of the feedback loop (Fig. 4) gives the key closed-loop transfer functions:

$$\text{Complementary sensitivity,}\quad r' \to \text{HR:}\quad T_o(s) = \frac{CP_o}{1+CP_o} = \frac{B_oG}{A_oH + B_oG}; \tag{10}$$

$$\text{Sensitivity,}\quad d \to \text{HR:}\quad S_o(s) = \frac{1}{1+CP_o} = \frac{A_oH}{A_oH + B_oG}; \tag{11}$$

$$\text{Input sensitivity,}\quad d \to v,\quad r' \to v\text{:}\quad U_o(s) = \frac{C}{1+CP_o} = \frac{A_oG}{A_oH + B_oG}, \tag{12}$$

from which the closed-loop characteristic polynomial Φ can be identified as

$$\Phi = A_oH + B_oG = A_osH' + B_oG. \tag{13}$$

A major algebraic-structural simplification can be obtained by using compensator zeros to cancel stable, well-damped plant poles (cf. [20]); the cancelled plant poles are then not shifted by the feedback and become poles of the closed-loop system. In this spirit, we constrain the compensator numerator to be $G = A_oG'$. The compensator transfer function (9) then specialises to

$$C(s) = \frac{A_oG'(s)}{sH'(s)}, \quad n_a + n_{g'} < n_{h'} + 1 \tag{14}$$

and the characteristic polynomial to $\Phi = A_osH' + B_oA_oG'$. Thus, for a solution to exist, A_o must be a factor of Φ, $\Phi = A_o\Phi'$, showing explicitly that the cancelled plant poles become poles of the closed-loop system, and the reduced characteristic polynomial Φ' is obtained as

$$\Phi' = sH' + B_oG'. \tag{15}$$

For a unique algebraic solution based on equating coefficients on either side of (15), the total number of unknown coefficients in G' and H', $n_{h'} + n_{g'} + 1$ (recall, H is monic), must be set equal to the degree of (15), which is $n_{\phi'} = n_{h'} + 1$ (the degree of sH', because of the strictly proper condition on P_o and C). Thus $n_{h'} + n_{g'} + 1 = n_{h'} + 1$, giving the solution $n_{g'} = 0$, that is G' is simply a constant, $G'(s) = g'_0$.

The strict-proper constraint for the compensator in (14) allows $n_a + n_{g'} = n_{h'}$ as one possible solution, viz. the solution giving H with minimal degree. Since from above $n_{g'} = 0$, $n_{h'} = n_a$ follows. The compensator structure is therefore

$$C(s) = \frac{A_og'_0}{sH'(s)}, \quad n_{h'} = n_a \tag{16}$$

where g'_0 and H' are obtained in general as the unique solution of (15) with $n_{\phi'} = n_{h'} + 1 = n_a + 1$, $n_{h'} = n_a$ and $n_{g'} = 0$.

Attention now turns to the structure of the input sensitivity function U_o which, from (12), generally has the form

$$d \to v\text{:}\quad U_o(s) = \frac{A_oG}{\Phi}. \tag{17}$$

As noted above, cancellation of plant poles using $G = A_oG'$ results in $\Phi = A_o\Phi'$ and consequently U_o can be simplified to

$$U_o = \frac{A_o^2G'}{A_o\Phi'} = \frac{A_oG'}{\Phi'}. \tag{18}$$

This form shows that an additional major simplification in the structure of U_o can be obtained by placing a further set of closed-loop poles at the location of the open-loop poles, which is achieved by including A_o as a factor of Φ'. Since $n_{\phi'} = n_a + 1$, Φ' is then allowed to contain just one further pole; setting $\Phi' = (s+p)A_o$, where p is real, the input sensitivity function simplifies down to the following first-order transfer-function:

$$U_o = \frac{G'}{(s+p)}. \tag{19}$$

Since, from above, $G' = g'_0$ ($n_{g'} = 0$), the final form for U_o is

$$U_o = \frac{g'_0}{(s+p)}. \tag{20}$$

The gain of this first-order transfer function, $|U_o(j\omega)|$, is, as desired, monotonically decreasing with frequency and cannot therefore have any peaking. It has a bandwidth equal to p [rad/s]. The coefficient $g'_0 = G'$ is obtained, as noted above, as the unique solution of (15) with $\Phi' = (s+p)A_o$ (thus $n_{\phi'} = n_a + 1$) and $n_{h'} = n_a$.

4.2. First order case

Proceeding on the assumption of a first-order plant

$$P_o(s) = \frac{B_o(s)}{A_o(s)} = \frac{k}{\tau s + 1} = \frac{k/\tau}{s + (1/\tau)}, \tag{21}$$

i.e. $n_a = 1$, we obtain $n_{h'} = 1$ and the final compensator structure can be written with $n_{g'} = 0$, $n_{h'} = 1 \Rightarrow G' = g'_0$, $H' = s + h'_0$ as

$$C(s) = \frac{A_oG'(s)}{sH'(s)} = \frac{(s + (1/\tau))g'_0}{s(s + h'_0)}. \tag{22}$$

An explicit, unique solution of (15) ($sH' + B_oG' = \Phi'$) can be obtained by noting that $n_{\phi'} = n_a + 1 = 2$, therefore $\Phi'(s) = s^2 + \phi'_1 s + \phi'_0$, and writing

$$s(s + h'_0) + \frac{k}{\tau}\cdot g'_0 = s^2 + \phi'_1 s + \phi'_0 \tag{23}$$

to give

$$h'_0 = \phi'_1, \quad g'_0 = \frac{\tau}{k}\cdot\phi'_0. \tag{24}$$

With $A_o = s + (1/\tau)$, $\Phi' = (s+p)A_o$ is

$$\Phi' = (s+p)\left(s + \frac{1}{\tau}\right) = s^2 + \left(p + \frac{1}{\tau}\right)s + \frac{p}{\tau}. \tag{25}$$

Thus,

$$\phi'_1 = p + \frac{1}{\tau}, \quad \phi'_0 = \frac{p}{\tau} \tag{26}$$

and, from (24), the controller coefficients h'_0 and g'_0 are obtained directly in terms of the given plant parameters k and τ and the bandwidth parameter p:

$$h'_0 = \phi'_1 = p + \frac{1}{\tau}, \quad g'_0 = \frac{\tau}{k}\cdot\phi'_0 = \frac{p}{k}. \tag{27}$$

Substituting for h'_0 and g'_0 in (22), the compensator becomes

$$C(s) = \frac{(s + (1/\tau))\cdot(p/k)}{s(s + p + (1/\tau))} \tag{28}$$

and, using (20), the input sensitivity function is

$$U_o = \frac{g'_0}{(s+p)} = \frac{(p/k)}{(s+p)} = \frac{(1/k)}{(1/p)\cdot s + 1}, \tag{29}$$

i.e. it is a first-order transfer function with steady-state gain $1/k$ and bandwidth p. With (28) and (29), the compensator and input-sensitivity transfer functions are seen to depend only on the nominal plant parameters k and τ, and on the input-sensitivity bandwidth parameter p.

4.3. Bandwidth selection

The special and simple structure of the input sensitivity function in Eq. (29) allows the bandwidth parameter p to be set according to a desired gain of U_o at some critical frequency.

From (29), the magnitude of U_o may be written

$$|U_o(j\omega)| = \frac{p/k}{(\omega^2 + p^2)^{1/2}}. \tag{30}$$

This can readily be solved to obtain an explicit expression for p:

$$p = \frac{\omega}{((1/(k|U_o(j\omega)|)^2) - 1)^{1/2}}. \tag{31}$$

Defining a critical frequency ω_c and a corresponding critical gain g_c, i.e. $g_c \triangleq |U_o(j\omega_c)|$, the desired input-sensitivity bandwidth p is

$$p = \frac{\omega_c}{((1/(kg_c)^2) - 1)^{1/2}}. \tag{32}$$

4.4. Algorithm summary

The steps involved in calculation of the compensator transfer function can now be summarised as follows:

1. Given data: nominal plant $P_o = k/(\tau s + 1)$ with steady-state gain k and time constant τ, Eq. (21).
2. Choose critical frequency and gain parameters, ω_c and g_c, and calculate input-sensitivity bandwidth parameter as $p = \omega_c/((1/(kg_c)^2) - 1)^{1/2}$, Eq. (32).
3. Implement feedback compensator as $C(s) = (s + (1/\tau)) \cdot (p/k)/(s(s + p + (1/\tau)))$, Eq. (28).

4.5. Controller calculation

Two controllers, denoted C_1 and C_2, were designed and tested based on the approximate nominal plant model Eq. (1):

$$P_o = \frac{k}{\tau s + 1} = \frac{24.2}{57.6s + 1} = \frac{0.420}{s + 0.0174}.$$

As discussed in Section 2, the critical gain and frequency values given by $|U_{o1}|_{f=0.01} = 0.0174$ were selected for controller C_1. Controller C_2 was designed to have +4 dB of gain at the same critical frequency.

Controller 1 ($C_1(s)$):

1. Given data: the nominal plant, above, has steady-state gain $k = 24.2$ bpm/(m/s) and time constant $\tau = 57.6$ s.
2. Choose critical frequency and gain parameters: $\omega_c = 0.0628$ rad/s ($= 2\pi \cdot 0.01 \equiv 0.01$ Hz) and $g_{c1} = 0.0174$ (m/s)/bpm ($\equiv -35.19$ dB). Calculate input-sensitivity bandwidth parameter as $p_1 = 0.0292$, Eq. (32).
3. Implement feedback compensator as in Eq. (28):

$$C_1(s) = \frac{0.00121(s + 0.0174)}{s(s + 0.0465)}. \tag{33}$$

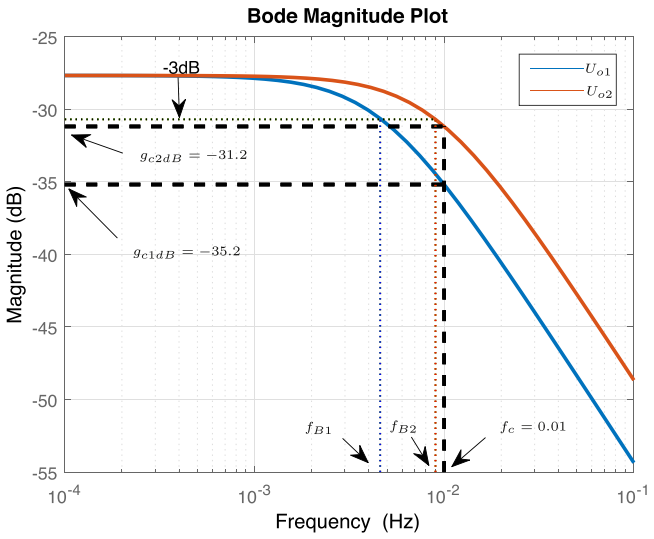

Fig. 6. Input sensitivity function magnitude $|U_o(j\omega)|$ for controllers C_1 (U_{o1}) and C_2 (U_{o2}), where C_2 was designed to have a gain of +4 dB at the chosen critical frequency f_c. The latter is shown as $f_c = 0.01$ Hz ($\equiv \omega_c = 0.0628$ rad/s). The critical gains g_c for C_1 and C_2 are shown in dB as g_{c1dB} and g_{c2dB}, respectively. Bandwidth: the vertical blue dotted line marks the bandwidth of U_{o1} at $f_{B1} = 0.0046$ Hz; the vertical red dotted line marks the bandwidth of U_{o2} at $f_{B2} = 0.0090$ Hz; the horizontal black dotted line marks the associated gain reduction of -3 dB with respect to the steady-state gain. (For interpretation of the references to colour in this legend, the reader is referred to the web version of the article.)

For this compensator, the corresponding input sensitivity function is, (29),

$$U_{o1} = \frac{0.00121}{(s + 0.0292)} = \frac{0.0413}{34.3s + 1}. \tag{34}$$

This transfer function (Fig. 6) has steady-state gain $1/k = 0.0413$ (m/s)/bpm ($\equiv -27.7$ dB) and bandwidth $p_1 = 0.0292$ rad/s ($\equiv f_{B1} = 0.0046$ Hz).

Controller 2 ($C_2(s)$):

The second controller, C_2, was designed to have a substantially higher bandwidth than C_1: the critical frequency for U_o was kept the same, but the critical gain at this frequency was increased by 4 dB (i.e. by an absolute factor of 1.5849).

1. Given data: the same nominal plant as above with $k = 24.2$ and $\tau = 57.6$.
2. Choose critical frequency and gain parameters: $\omega_c = 0.0628$ rad/s (as above) and $g_{c2} = 0.0174 \times 1.5849 = 0.0276$ (m/s)/bpm ($\equiv -35.19 + 4 = -31.19$ dB). Calculate input-sensitivity bandwidth parameter as $p_2 = 0.0563$, Eq. (32).
3. Implement feedback compensator as in Eq. (28):

$$C_2(s) = \frac{0.00233(s + 0.0174)}{s(s + 0.0737)}. \tag{35}$$

The input sensitivity function is in this case, (29),

$$U_{o2} = \frac{0.00233}{(s + 0.0563)} = \frac{0.0413}{17.8s + 1}. \tag{36}$$

This input-sensitivity function (Fig. 6) has the same steady-state gain as for controller 1, that is to say $1/k = 0.0413$ (-27.7 dB), but a bandwidth $p_2 = 0.0563$ rad/s ($\equiv f_{B2} = 0.0090$ Hz) which is approximately twice that for controller 1 (cf. Eqs. (34) and (36)), i.e. $0.0563/0.0292 = 1.93$.

The frequency responses of the two input sensitivity functions, U_{o1} and U_{o2}, can conveniently be visualised and compared in a Bode plot (Fig. 6).

Table 2
Principal outcome measures for overall evaluation of C_1.

	Mean (SD)	95% CI	Range
RMSE/(bpm)	2.96 (0.85)	2.65–3.28	1.40–4.58
$P_{\Delta v}/(10^{-4}\,\mathrm{m^2/s^2})$	16.00 (1.41)	15.47–16.52	14.05–19.94

$n = 30$.
SD: standard deviation.
95% CI: 95% confidence interval for the mean.
RMSE: root-mean-square tracking error; $P_{\Delta v}$: average power of changes in v; bpm: beats per minute.

5. Results

Controller C_1 gave highly accurate, stable and robust overall performance for all 30 subjects tested, with a mean RMS tracking error of 2.96 bpm and a 95% confidence interval for the mean RMSE of 2.65–3.28 bpm (Table 2). The control signal v, i.e. the treadmill speed reference, was stable and acceptably smooth in all tests; the average power of changes in v was $16.00 \times 10^{-4}\,\mathrm{m^2/s^2}$ (95% CI: $15.47–16.52 \times 10^{-4}\,\mathrm{m^2/s^2}$). In addition to these quantitative outcomes, the control performance for C_1 can be qualitatively assessed by inspection of heart rate HR and control signal v for the tests with the lowest, median and highest RMSE values (Fig. 7).

Comparison between the performance of C_1 for the non-identified subject group ("C_1 no ID") and for the matched subgroup of subjects who had participated in the identification study ("C_1 ID") showed no significant difference in tracking accuracy – mean RMSE 2.69 vs. 3.28 bpm, C_1 no ID vs. C_1 ID, $p = 0.24$ — or average control signal power – mean $P_{\Delta v}$ 15.62 vs. $16.31 \times 10^{-4}\,\mathrm{m^2/s^2}$, C_1 no ID vs. C_1 ID, $p = 0.37$ – (Table 3, upper rows; C_1 no ID vs. C_1 ID; Fig. 8).

Controller C_2, which was purposely designed with +4 dB of gain at the critical frequency ω_c, showed significantly higher average control signal power (mean $P_{\Delta v}$ 18.54 vs. $16.00 \times 10^{-4}\,\mathrm{m^2/s^2}$, C_2 vs. C_1, $p = 0.0012$) and modest evidence of more accurate tracking (lower mean RMSE of 2.71 vs. 2.95 bpm, C_2 vs. C_1, $p = 0.062$) than C_1 (Table 3, middle rows; C_2 vs. C_1; Fig. 8).

Examination and comparison of the steady-state performance of C_1 during the early time interval of $300 \le t \le 600$ and the later time interval of $1800 \le t \le 2100$ showed substantial and significant improvement in tracking accuracy (decrease in mean RMSE from 2.88 to 2.17 bpm, $p < 0.001$) and a significant reduction in average control signal power (mean $P_{\Delta v}$ 2.09 vs. $1.40 \times 10^{-4}\,\mathrm{m^2/s^2}$, $p = 0.0030$) over time (Table 3, lower rows; Fig. 8).

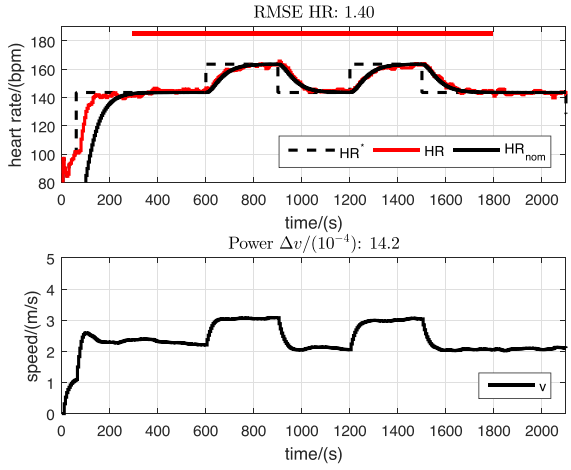

(a) Subject S26, lowest RMSE of 1.40 bpm, $P_{\Delta v} = 14.2 \times 10^{-4}\,\mathrm{m^2/s^2}$. $\mathrm{HR}^* = 153.6 \pm 10$ bpm.

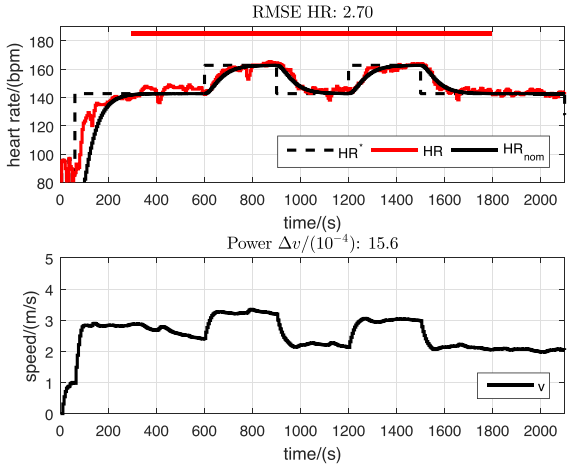

(b) Subject S33, median RMSE of 2.70 bpm, $P_{\Delta v} = 15.6 \times 10^{-4}\,\mathrm{m^2/s^2}$. $\mathrm{HR}^* = 152.8 \pm 10$ bpm.

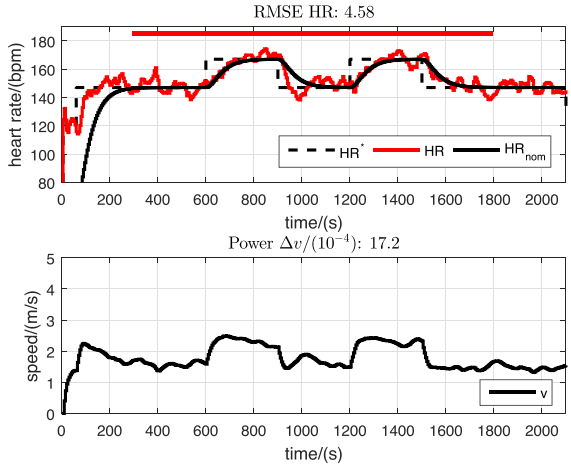

(c) Subject S22, highest RMSE of 4.58 bpm, $P_{\Delta v} = 17.2 \times 10^{-4}\,\mathrm{m^2/s^2}$. $\mathrm{HR}^* = 157.0 \pm 10$ bpm.

Fig. 7. Results with C_1 with the lowest (a), median (b) and highest (c) values for RMS tracking error. In the upper part of each figure, HR^* is the heart rate reference, $\mathrm{HR_{nom}}$ is the target nominal heart rate response (simulated), and HR is the measured heart rate. In the lower graphs, v is the control signal, i.e. the treadmill speed reference. RMSE: root-mean-square tracking error, Eq. (5). $P_{\Delta v}$: average control signal power, Eq. (6).

Table 3
Principal outcome measures for paired comparisons and p-values for comparison of means.

	Mean (SD)		MD (95 % CI)	n	p-Value
	C_1 no ID	C_1 ID			
RMSE/(bpm)	2.69 (0.99)	3.28 (0.88)	−0.59 (−1.66,0.48)	10	0.24
$P_{\Delta v}/(10^{-4}\,\mathrm{m}^2/\mathrm{s}^2)$	15.62 (1.76)	16.31 (1.33)	−0.69 (−2.33,0.95)	10	0.37
	C_2	C_1			
RMSE/(bpm)	2.71 (0.61)	2.95 (0.83)	−0.24 (−0.55,0.08)	10	0.062
$P_{\Delta v}/(10^{-4}\,\mathrm{m}^2/\mathrm{s}^2)$	18.54 (3.10)	16.00 (1.75)	2.55 (1.17,3.92)	10	0.0012
	C_1, $300 \le t \le 600$	C_1, $1800 \le t \le 2100$			
RMSE/(bpm)	2.88 (0.93)	2.17 (1.00)	0.71 (0.34,1.07)	30	4.4×10^{-4}
$P_{\Delta v}/(10^{-4}\,\mathrm{m}^2/\mathrm{s}^2)$	2.09 (1.66)	1.40 (1.51)	0.69 (0.08,1.30)	30	0.0030

SD: standard deviation.
MD: mean difference.
95% CI: 95% confidence interval for the mean difference.
p-values are: for C_1 no ID vs. C_1 ID, paired two-sided t-test; for C_2 vs. C_1, paired one-sided t-test; for C_1(300–600) vs. C_1(1800–2100), paired two-sided t-test (RMSE) and paired two-sided Wilcoxon signed rank test ($P_{\Delta v}$).
RMSE: root-mean-square tracking error; $P_{\Delta v}$: average power of changes in v; bpm: beats per minute.

Comparison of tracking error and average control signal power during the dynamic changes of the four individual steps 1–4 showed significant differences in RMSE (overall p-value of $p = 0.0036$) but no significant difference in $P_{\Delta v}$ (overall, $p = 0.14$) over time; (Table 4, Fig. 9). Proceeding to post-hoc pairwise comparisons of RMSE for the individual steps, modest evidence was found for a reduction between steps 1 and 2 (mean RMSE 3.31 vs. 2.69 bpm, $p = 0.051$), while significant reductions were found between steps 1 and 3 (3.31 vs. 2.77 bpm, $p = 0.017$), and 1 and 4 (3.31 vs. 2.59 bpm, $p = 0.027$). No other paired comparisons for RMSE showed a significant difference.

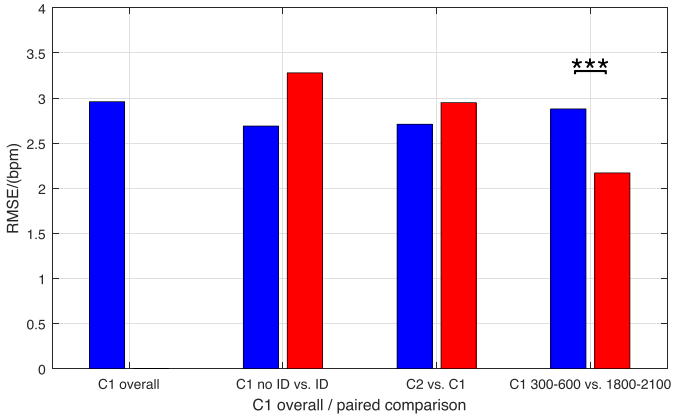

(a) RMS tracking error, RMSE.

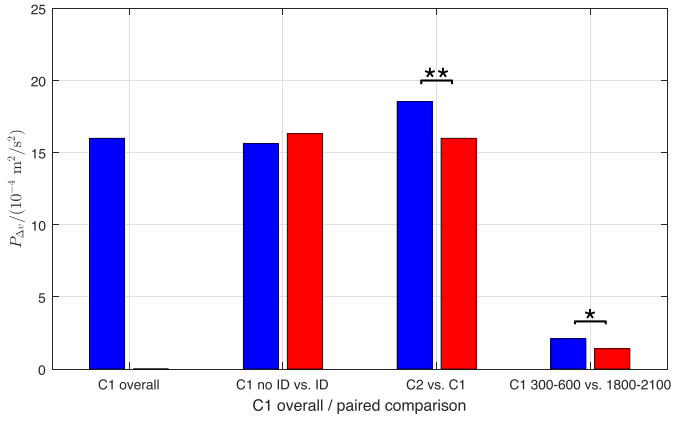

(b) Average control signal power, $P_{\Delta v}$.

Fig. 8. Mean values of principal outcome measures for paired comparisons (cf. Table 3), with significance indicators: $^{*}\Leftrightarrow p < 0.05$; $^{**}\Leftrightarrow p < 0.01$; $^{***}\Leftrightarrow p < 0.001$. The overall outcomes for C_1 are included for reference only.

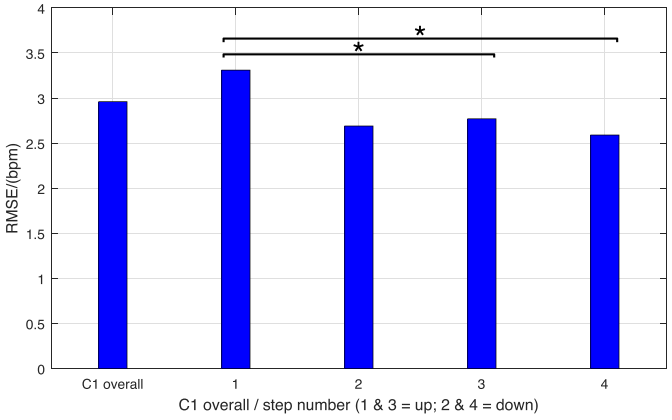

(a) RMS tracking error, RMSE. Overall $p = 0.0036$.

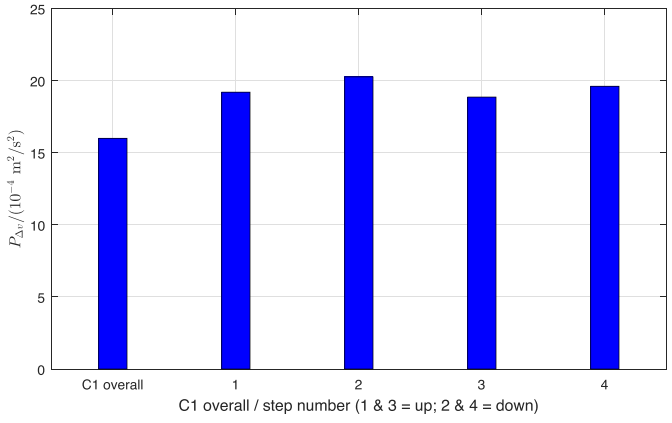

(b) Average control signal power, $P_{\Delta v}$. Overall $p = 0.14$.

Fig. 9. Mean values of principal outcome measures for individual steps 1–4 (cf. Table 4), with significance indicators for paired comparisons on RMSE: $^{*}\Leftrightarrow p < 0.05$. The overall outcomes for C_1 are included for reference only.

Table 4
Outcomes for individual steps with C_1.

	Mean (SD) Step number				p-Value
	1	2	3	4	
RMSE/(bpm)	3.31 (1.35)	2.69 (0.80)	2.77 (1.11)	2.59 (0.84)	0.0036
$P_{\Delta\nu}/(10^{-4}\,m^2/s^2)$	19.20 (2.60)	20.26 (2.63)	18.86 (2.67)	19.61 (2.45)	0.14

p-values for post-hoc pairwise comparisons on RMSE: 1 vs. 2, $p = 0.051$; 1 vs. 3, $p = 0.017$; 1 vs. 4, $p = 0.027$; all other paired comparisons not significant.
$n = 29$ (S22 excluded, see Section 3.6).
Steps 1 and 3: up; steps 2 and 4: down.
Values for RMSE and $P_{\Delta\nu}$ calculated over 300-s after step onset.
SD: standard deviation.
RMSE: root-mean-square tracking error; $P_{\Delta\nu}$: average power of changes in ν; bpm: beats per minute.

6. Discussion

This research work had two main objectives: to develop a new method for feedback control of heart rate during treadmill exercise based on shaping of the input sensitivity function, and to empirically evaluate quantitative performance outcomes with the proposed method in an experimental study. The control approach was motivated by the principal design issue of achieving a suitable degree of disturbance rejection of very-low-frequency heart rate variability, while maintaining a level of control signal activity which is sufficiently smooth and acceptable to the runner.

The control design method was found meet the disturbance rejection and control signal requirements: controller C_1 was robust across all 30 subjects tested; overall heart rate tracking performance was accurate with a mean RMSE of ∼3 bpm; and the control signal (treadmill speed) was very smooth with a low average power on a tight range of ∼14–20 m^2/s^2 across all subjects. The ability of the input sensitivity function to absorb a substantial degree of inter-subject differences in HRV is most strikingly apparent when considering the results with C_1 with the lowest, median and highest RMS tracking errors (Fig. 7). Subject S26 (lowest RMSE of 1.40 bpm, Fig. 7(a)) is clearly an individual with intrinsically low HRV, while subject S22, in contrast, has high-amplitude HRV, leading to the highest RMSE of 4.58 bpm (Fig. 7(c)), a factor of ∼3.3 higher than that for S26. Despite this wide range of HRV magnitudes, the average control signal power and its qualitative behaviour remained satisfactory throughout, with $P_{\Delta\nu}$ on the proportionately narrow range of 14.2–17.2 $\times 10^{-4}\,m^2/s^2$ for these three subjects, namely the subjects with the "best," "middle" and "worst" tracking performance.

The design method guarantees that the nominal input sensitivity function U_o has a gain which is monotonically decreasing with frequency, is therefore devoid of peaking, and which takes on a pre-specified and desirable value at a chosen critical frequency: the only design parameters which have to be chosen are the critical gain and frequency; calculation of the controller parameters is then explicit and straightforward. The empirical comparison of two different controllers, C_1 and C_2, demonstrated that tuning of these parameters to modify the tradeoff between performance outcomes is clear and simple: controller C_2, with +4 dB of gain in $|U_o|$ at a common critical frequency, delivered more accurate tracking at the cost of higher average control signal power.

It was hypothesised at the outset that parametric and/or structural uncertainty in the plant play only a secondary role in heart rate control systems: the nominal plant model assumed here was a linear time-invariant (LTI) first-order system whose parameters were obtained as average values from a previous system identification study [13]; the input-sensitivity-shaping design approach thus used a single approximate nominal plant model, and did not require any information on, or identification of, heart rate dynamics for individual participants in the present work. The experimental comparison of the identified and non-identified subject groups showed no significant differences in performance outcomes, thus lending support to the proposal that a very approximate and simple LTI plant model is sufficient to achieve accurate, stable and robust heart rate control performance.

The analysis of control loop performance over time showed a tendency for both RMS tracking error and average control signal power to decrease: the early vs. late regulation comparison showed substantial and significant reductions in both RMSE and $P_{\Delta\nu}$ in the later time interval; and the dynamic tracking analysis for individual steps showed that RMSE decreased significantly over time. There are two possible explanations for these observations. First, analysis of all test results from this study indicates that the amplitude of the HRV disturbance generally decreases as the exercise progresses, presumably due to on-going physiological adaptations in body temperature, fatigue level etc. This reduction in disturbance amplitude will naturally lead to more accurate tracking and lower control signal power. Second, changes in performance will also be attributable in part to variations in plant parameters over time. The preceding identification study, [13], reported a significant reduction in steady-state gain k over time: k had the relatively high value of ∼33 bpm/(m/s) in the early stage of exercise (after 10–15 min), but this value was observed to reduce rapidly towards the overall nominal value of ∼24 bpm/(m/s) with continuing exercise. This pattern of change in plant gain would lead to an increase in the gain of the input sensitivity function (the steady-state gain of U_o is $1/k$, Eq. (29)) thus, theoretically, giving a higher loop bandwidth and, correspondingly, a reduction in RMS tracking error and an increase in control signal power. Since only the former change was seen in the experimental results (i.e. lower RMSE), it can be concluded that reduction in HRV amplitude over time is the primary mechanism leading to simultaneously lower RMS tracking error and average control signal power; the effects of changes in plant gain are apparently secondary.

7. Conclusions

The empirical results obtained in this study strongly support the concept that the principal design issue for feedback control of heart rate is disturbance rejection behaviour in relation to very-low-frequency heart rate variability. There is a strong degree of intra-subject and inter-subject inconstancy in observed heart rate variability: the HRV is itself highly variable.

The input-sensitivity-shaping method provides a direct and straightforward way to address this design challenge, leading to robust and accurate tracking and to a smooth, low-power control signal.

Issues of parametric and structural plant uncertainty appear to play a secondary and indeed minor role, because the results obtained here were achieved using a simple approximate plant model which was not specific to any of the subjects tested.

Authors' contributions

KH designed the study. SF did the data acquisition. KH and SF contributed to the analysis and interpretation of the data. KH wrote the manuscript; SF revised it critically for important intellectual content. Both authors read and approved the final manuscript.

Competing interests

The authors declare that they have no competing interests.

References

[1] L.S. Pescatello, R. Arena, D. Riebe, P.D. Thompson (Eds.), ACSM's Guidelines for Exercise Testing and Prescription, 9th ed., Lippincott, Williams and Wilkins, Philadelphia, USA, 2014.
[2] C.E. Garber, B. Blissmer, M.R. Deschenes, B.A. Franklin, M.J. Lamonte, I.-M. Lee, D.C. Nieman, D.P. Swain, American College of Sports Medicine position stand. Quantity and quality of exercise for developing and maintaining cardiorespiratory, musculoskeletal, and neuromotor fitness in apparently healthy adults: guidance for prescribing exercise, Med. Sci. Sports Exerc. 43 (7) (2011) 1334–1359.
[3] M. Weston, K.L. Taylor, A.M. Batterham, W.G. Hopkins, Effects of low-volume high-intensity interval training (HIT) on fitness in adults: a meta-analysis of controlled and non-controlled trials, Sports Med. 44 (7) (2014) 1005–1017.
[4] J.S. Ramos, L.C. Dalleck, A.E. Tjonna, K.S. Beetham, J.S. Coombes, The impact of high-intensity interval training versus moderate-intensity continuous training on vascular function: a systematic review and meta-analysis, Sports Med. 45 (5) (2015) 679–692.
[5] A. Mezzani, L.F. Hamm, A.M. Jones, P.E. McBride, T. Moholdt, J.A. Stone, A. Urhausen, M.A. Williams, Aerobic exercise intensity assessment and prescription in cardiac rehabilitation, Eur. J. Prev. Cardiol. 20 (3) (2013) 442–467.
[6] G.E. Billman, Heart rate variability – a historical perspective, Front. Physiol. 2 (86) (2011).
[7] M. Malik, et al., Heart rate variability. Standards of measurement, physiological interpretation, and clinical use, Eur. Heart J. 17 (3) (1996) 354–381.
[8] R. Sassi, S. Cerutti, F. Lombardi, M. Malik, H.V. Huikuri, C.K. Peng, G. Schmidt, Y. Yamamoto, Advances in heart rate variability signal analysis, Europace 17 (9) (2015) 1341–1353.
[9] S.W. Su, L. Wang, B.G. Celler, A.V. Savkin, Y. Guo, Identification and control for heart rate regulation during treadmill exercise, IEEE Trans. Biomed. Eng. 54 (7) (2007) 1238–1246.
[10] T.M. Cheng, A.V. Savkin, B.G. Celler, S.W. Su, L. Wang, Nonlinear modeling and control of human heart rate response during exercise with various work load intensities, IEEE Trans. Biomed. Eng. 55 (11) (2008) 2499–2508.
[11] S. Scalzi, P. Tomei, C.M. Verrelli, Nonlinear control techniques for the heart rate regulation in treadmill exercises, IEEE Trans. Biomed. Eng. 59 (3) (2012) 599–603.
[12] T.N. Nguyen, S. Su, B. Celler, H. Nguyen, Advanced portable remote monitoring system for the regulation of treadmill running exercises, Artif. Intell. Med. 61 (2) (2014) 119–126.
[13] K.J. Hunt, S.E. Fankhauser, J. Saengsuwan, Identification of heart rate dynamics during moderate-to-vigorous treadmill exercise, Biomed. Eng. Online 14 (2015) 117.
[14] K.J. Hunt, A.J.R. Hunt, Feedback control of heart rate during outdoor running: a smartphone implementation, Biomed. Signal Process. Control 26 (2016) 90–97.
[15] K.J. Hunt, R.R. Maurer, Comparison of linear and nonlinear feedback control of heart rate for treadmill running, Syst. Sci. Control Eng. 4 (1) (2016) 87–98.
[16] K.J. Åström, B. Wittenmark, Computer Controlled Systems: Theory and Design, 3rd ed., Dover Publications, Mineola, New York, USA, 2011.
[17] H. Kwakernaak, Robust control and $\mathcal{H}_\infty$-optimisation – tutorial paper, Automatica 29 (2) (1993) 255–273.
[18] N.S. Nise, Control Systems Engineering, 3rd ed., Wiley, New York, USA, 2000.
[19] E. Shargal, R. Kislev-Cohen, L. Zigel, S. Epstein, R. Pilz-Burstein, G. Tenenbaum, Age-related maximal heart rate: examination and refinement of prediction equations, J. Sports Med. Phys. Fit. 55 (10) (2015) 1207–1218.
[20] K.J. Åström, R.M. Murray, Feedback Systems, Princeton University Press, Princeton, USA/Oxford, UK, 2008.